Supporting Information

Giridhar et al. 10.1073/pnas.1015165108

SI Text

By construction, correlation coefficients have chance correlation removed, thus correcting for any expected rate-dependent effects (but see refs. 1 and 2). However, decoding neurons are likely sensitive to absolute differences in spike time covariability or firing rates, regardless of whether these events occur above or below chance. To evaluate possible changes in joint spike train activity without regard for changes in rate, we also calculated timescale-dependent *coincidence* (*SI Materials and Methods*). Inhibition-evoked changes in coincidence were qualitatively and quantitatively similar to the observed changes in correlation (peak increases, 0.012 ± 0.004; peak decreases, 0.012 ± 0.01; Fig. S1 *B* and *C*). Whereas downstream neurons may be sensitive to multiple measures of input similarity, our timescale-dependent changes are not strongly metric dependent and are observed using multiple definitions of similarity.

SI Materials and Methods

Slice Preparation. All procedures were done in accordance with the guidelines for the care and use of animals at Carnegie Mellon University and as previously described (3–5). C57BL/6 mice (age P14–P20) were anesthetized using isofluorane. Anesthesia was monitored by responsiveness to tail pinch and animals were decapitated. Dissection and slicing were both performed in ice-cold Ringer's solution (125 mM NaCl, 25 mM glucose, 2.5 mM KCl, 25 mM $NaHCO_3$, 1.25 mM NaH_2PO_4, 1 mM $MgCl_2$, and 2.5 mM $CaCl_2$). Coronal or sagittal slices (300–350 μm) were obtained from the olfactory bulb using a vibratome (VT1000S; Leica). Slices were placed in oxygenated Ringer's solution at 37 °C for 15 min and then allowed to recover for 30 min before being used for electrophysiology.

Electrophysiology. Data were recorded using software written in Igor Pro (WaveMetrics) with a 700B amplifier (Molecular Devices) and an ITC-18 data acquisition board (InstruTech). Whole-cell patch pipettes (1–3 MΩ) with internal solution (130 mM potassium gluconate, 10 mM Hepes, 2 mM $MgCl_2$, 2 mM MgATP, 2 mM Na_2ATP, 0.3 mM GTP, and 4 mM NaCl) were used to make whole-cell current-clamp recordings. Because granule cells are typically quiescent in slice preparations (due to fewer active mitral cell inputs), we increased granule cell excitability either by reducing magnesium concentration in the extracellular solution to 0.2 mM (6) or by using standard Ringer's solution with 10 μM (*S*)-3,5-dihydroxyphenylglycine (DHPG), an mGluR agonist that increases granule cell excitability (5, 7) (Fig. S1). DHPG has previously been shown to increase the rate of spontaneous inhibitory events without changing the waveforms of IPSCs (5). Experiments were performed at 37 °C.

Stimulus currents were defined by a DC offset (50–1,000 pA) applied for 2,000 ms to evoke mitral cell firing. This current injection elicited a range of firing rates across pairs (6–55 Hz). The amplitude of the injected current was set so that firing rates in the two cells were roughly equal. We discarded sweeps in which firing rate was >2 SD from average, as these changes are likely due to random spontaneous activity rather than evoked inhibition. We also excluded pairs whose apical dendrites terminated in the same glomerulus, as these pairs have additional forms of excitatory and inhibitory coupling that are not the focus of this paper (one pair excluded, Fig. S3). Because we wanted to include pairs in which the effects of inhibition were observable, we included pairs displaying at least some slow decorrelation as this effect has already been shown to be inhibition mediated in this preparation (3). As mentioned above, we used two methods to increase granule cell excitability: reduced Mg^{2+} concentration or DHPG. We found that the spontaneous rate of IPSCs in the DHPG experiments was consistent over time whereas low magnesium often caused the spontaneous rate of inhibition to fluctuate at very slow timescales (thus increasing long timescale correlation: Fig. S1*F*, blue trace). For this reason, more low-Mg^{2+} pairs (10/13) than DHPG pairs (3/11) were excluded from analysis. All data (including excluded pairs) can be seen in Fig. S1*F*.

Data Analysis. Firing rates were measured over 2-s periods across repeated trials (20–80). Cross-timescale correlation was calculated by binning spike trains at bin sizes ranging from 1 to 1,000 ms and calculating correlation using the following equation. Synchrony was defined as correlation measured at a bin size of 10 ms:

$$\rho_T = \frac{\langle n_1 n_2 \rangle - \langle n_1 \rangle \langle n_2 \rangle}{\sqrt{\langle n_1^2 \rangle - \langle n_1 \rangle^2} \sqrt{\langle n_2^2 \rangle - \langle n_2 \rangle^2}}.$$

Coincidence was calculated by eliminating chance correction in the correlation formula

$$c_T = \frac{\langle n_1 n_2 \rangle}{\sqrt{\langle n_1^2 \rangle} \sqrt{\langle n_2^2 \rangle}}.$$

All P values noted were calculated using a t test.

Models: Two-Cell Network. All simulations were performed in Matlab. The two-cell model consists of two excitatory LIF neurons described by the equation

$$\tau_m \frac{\Delta V_i}{\Delta t} = -I_{stim} - I_{syn,I,i}(t) - I_{noise,i}(t) - I_{leak,i}(t),$$

Where τ_m is the membrane time constant (τ_m = 10 ms). For all simulations, the time step Δt = 0.01 ms and a standard Euler integration scheme were used. The stimulus (I_{stim}) was set at a constant for each cell (1.5 for cell 1, 1.6 for cell 2). Noise currents (I_{noise}) were uncorrelated across cells and were generated as the sum of two 100-Hz Poisson trains convolved with a time constant describing decay (τ_{noise} = 3 ms) and scaled by 0.3 for excitatory trains and −0.3 for inhibitory trains. Inhibition ($I_{syn,I}$) was modeled as pools of Poisson-rate inhibitory current delivered to the two excitatory cells. The correlation of inhibitory input was set by the parameter c, which set the portion of the inhibitory pool that was shared by the pair (the unshared portion is described by $1 - c$). Leak current (I_{leak}) = $g_L(V_i(t) - V_L)$, where g_L is the unitary leak current (g_L = 1) and V_L is the reversal potential of the leak term (V_L = 0).

When either of the excitatory cells was depolarized to threshold (V_{thresh} = 1), a spike was identified and the membrane potential was reset to V_{reset} = 0 for the duration of the refactory period ($t_{refract}$ = 5 ms). Spikes from either excitatory cell resulted in an α-function determining the time-varying Poisson rate, $P_{(-)}$ at which inhibitory pools were activated,

$$P_{(-)} = k \sum_{i=1}^{2} \sum_{j} \frac{t - t_{ij}}{\tau_\alpha} e^{\left(-(t-t_{ij})/\tau_\alpha\right)},$$

where t_{ij} is the jth spike time from the ith excitatory cell, k = 1, and τ_α = 2.5. Because inhibition should be bounded in any real

neural circuit, we convolved this activity-evoked probability by a hyperbolic tangent function to induce a saturation in the amount of available inhibition. This saturation was described by the equation

$$P_{(-),\text{conv}} = \frac{a}{2}\left(\tanh\left(2bP_{(-)} + d\right) + 1\right),$$

where a, b, and d are constants specific to shared and individual pools of inhibition (for unshared inhibitory pools, $a = 0.4$, $b = 30$, and $d = -3.5$; and for shared inhibitory pools, $a = 0.75$, $b = 65$, and $d = -5$). The resultant Poisson rate for each inhibitory pool is scaled by the proportion of shared inhibition such that

$$P_{(-),\text{indiv}} = (1-c)P_{(-),\text{conv}}$$

and

$$P_{(-),\text{shared}} = cP_{(-),\text{conv}}.$$

Inhibitory current delivered to mitral cells is also described by the α-function equation where $\tau_\alpha = 1.1$ and $k = -6.0$.

Network Model: Stimulus Generation. Stimuli applied to the network model were generated by randomly dividing the excitatory cells into two groups: group A and group B. For stimulus 1, group A was stimulated at a higher intensity 1 (11.5 ± 0.5), whereas group B was stimulated at a slightly lower intensity 2 (10.7 ± 0.5). For stimulus 2, group B was stimulated at the higher intensity and group A was stimulated at the lower intensity. For all cells, the initial value of the stimulation current was given a slight slope across time ($0.0002t$) to attain physiologically realistic values of pairwise correlation in the no-coupling scenario. Whether this source of slow correlation was a ramp or sinusoid did not impact results over our range of analyzed timescales.

Because we wanted to know how well an unbiased observer of the network could discriminate between stimuli, we again divided the network into two observation groups (unrelated to stimulus-defined groups A and B). Cells were assigned to observation group 1 or 2 with 50% probability and output patterns were quantified as the average firing rate in each group measured over 500-ms epochs. Pattern representations (Figs. 4 *E* and *F* and 5 *A* and *B*) were plotted using group 1/group 2 firing rate data collected over 150 trials.

Linear Discriminant and ROC Analysis. To quantify the degree to which stimuli 1 and 2 were discriminable via observation of groups 1 and 2, we used a linear discriminant and receiver–operator characteristic (ROC) analysis. For each model variant, we identified the plane along which stimulus 1 and stimulus 2 were most discriminable given the observed stimulus-evoked patterns (Figs. 4 *E* and *F* and 5 *A* and *B*). Briefly, we calculated the center of the stimulus 1 and stimulus 2 distributions in (x, y) coordinates and a line perpendicular to the line connecting the centers of stimulus 1 and stimulus 2 distributions was used as the plane of maximum discriminability. As this line was translated along the y axis, the numbers of true positive trials (α, correct identification of applied stimulus) and false positive (β) trials were counted. The discriminability metric (d) was calculated by integrating the area under each curve and subtracting 0.5 (because 0.5 corresponds to chance levels of identification) and multiplying by 2. Thus, d describes on a scale of 0–1 how well above chance the network's evoked responses are discriminable above chance.

Network Model. On the basis of the architecture of the mammalian olfactory bulb, our model consists of 900 current-based LIF neurons, 11% of which are excitatory and 89% of which are inhibitory. Excitatory and inhibitory cells are connected via reciprocal dendrodendritic synapses with a pairwise connection probability of 20%. The model lacks excitatory–excitatory and inhibitory–inhibitory connections. Each cell in the model obeyed the equation

$$\tau_\text{m}\frac{\Delta V_i}{\Delta t} = -g_\text{L}(V_i(t) - V_\text{L}) - I_{\text{syn,E},i}(t) - I_{\text{syn,I},i}(t) - I_{\text{noise},i}(t) - I_\text{stim},$$

where V_i is the membrane voltage of the ith neuron, τ_m is the membrane time constant (9.5 ± 0.5 ms), g_L is the unitary leak current (0.5), and V_L is the reversal potential of the leak term (−55 mV). $I_\text{syn,E}$ and $I_\text{syn,I}$ describe excitatory and inhibitory synaptic activity, respectively, arising from activation of synapses in the network. All synaptic currents were described by

$$\tau_x\frac{\Delta I_x}{\Delta t} = -I_{x,i},$$

where τ_x is the time constant describing the decay of synaptic excitatory or inhibitory input currents ($\tau_\text{E} = 3$ ms, $\tau_\text{I} = 3$ ms). When a cell's membrane potential reaches threshold ($V_\text{thresh} = -45.5 \pm 0.5$ mV), the neuron fires an action potential, a spike time is identified, and that neuron's membrane potential is reset to ($V_\text{reset} = -54.5 \pm 0.5$ mV). After being reset, the neuron remains refractory for a fixed amount of time, $t_\text{refract} = 5$ ms. The synaptic current received by the cell's postsynaptic targets is augmented by the equation

$$I_{x,i}(t) = I_{x,i}(t) + \Delta I_x,$$

where Δi_x is the unitary augmentation in synaptic current evoked by presynaptic activity. Unitary currents were adjusted slightly for each model variant to normalize amplitudes of correlation changes ($\text{OB}_{(-)}$:$\Delta i_\text{E} = 0.55$, $\Delta i_\text{E} = -0.82$; $\text{sync}_{(\pm)}$:$\Delta i_\text{E} = 0.35$, $\Delta i_\text{E} = -2.2$, $\text{async}_{(-)}$, $\Delta i_\text{E} = 0.65$, $\Delta i_\text{E} = -1.2$). Noise currents were uncorrelated across cells and were generated as the sum of two 100-Hz Poisson trains convolved with a time constant describing decay ($\tau_\text{noise} = 3$ ms) and scaled by 2.2 for excitatory trains and −2.2 for inhibitory trains. The sum of these trains is thought of as a barrage of uncorrelated excitatory and inhibitory synaptic input from sources external to our network (for example, inputs from olfactory receptor neurons, periglomerular cells, or centrifugal inputs from cortex). Finally, I_stim is a constant DC offset current delivered to neurons as described in *Network Model: Stimulus Generation* above ($I_\text{stim} = 10.7 \pm 0.5$ for group A and 11.5 ± 0.5 for group B). Spike trains generated by these models were analyzed using the same methods described above.

1. Kumar A, Rotter S, Aertsen A (2010) Spiking activity propagation in neuronal networks: Reconciling different perspectives on neural coding. *Nat Rev Neurosci* 11: 615–627.
2. Averbeck BB, Lee D (2006) Effects of noise correlations on information encoding and decoding. *J Neurophysiol* 95:3633–3644.
3. Arevian AC, Kapoor V, Urban NN (2008) Activity-dependent gating of lateral inhibition in the mouse olfactory bulb. *Nat Neurosci* 11:80–87.
4. Galán RF, Fourcaud-Trocmé N, Ermentrout GB, Urban NN (2006) Correlation-induced synchronization of oscillations in olfactory bulb neurons. *J Neurosci* 26:3646–3655.
5. Castro JB, Hovis KR, Urban NN (2007) Recurrent dendrodendritic inhibition of accessory olfactory bulb mitral cells requires activation of group I metabotropic glutamate receptors. *J Neurosci* 27:5664–5671.
6. Kapoor V, Urban NN (2006) Glomerulus-specific, long-latency activity in the olfactory bulb granule cell network. *J Neurosci* 26:11709–11719.
7. Dong HW, Hayar A, Ennis M (2007) Activation of group I metabotropic glutamate receptors on main olfactory bulb granule cells and periglomerular cells enhances synaptic inhibition of mitral cells. *J Neurosci* 27:5654–5663.

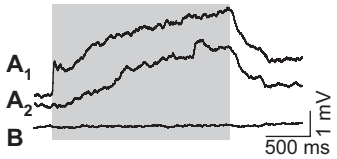

Fig. S1. Example of excitatory coupling between mitral cells. Traces show average change in membrane potential of the unstimulated cell during stimulation of the other cell in the pair. The stimulation period is shaded. (A_1 and A_2) Example from a homotypic pair. Excitatory coupling is evident, and this pair was excluded from analysis. (*B*) Average change across heterotypic pairs reported in this paper.

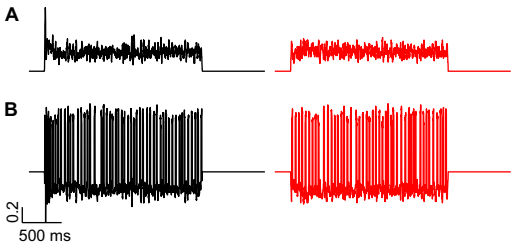

Fig. S2. Example of repeated patterns and transients. (*A*) Repeated patterns. Histograms of activity, time locked to current injection, are shown for one mitral pair (cell 1, black; cell 2, red). For some cells, repeated patterns include a robust transient after current injection onset (cell 1, black). Importantly, these transients are present in all trials—not just the together recording condition. The values of correlation that we report represent increases above any baseline level of correlation. (*B*) Unrepeated patterns. Unrepeated spike patterns can be described as the difference between a single binary spike train and the repeated pattern plotted above (example shown from the same pair). Unrepeated patterns (like the ones plotted here) exhibit timescale-dependent correlation changes only when the cells can receive shared local inputs.

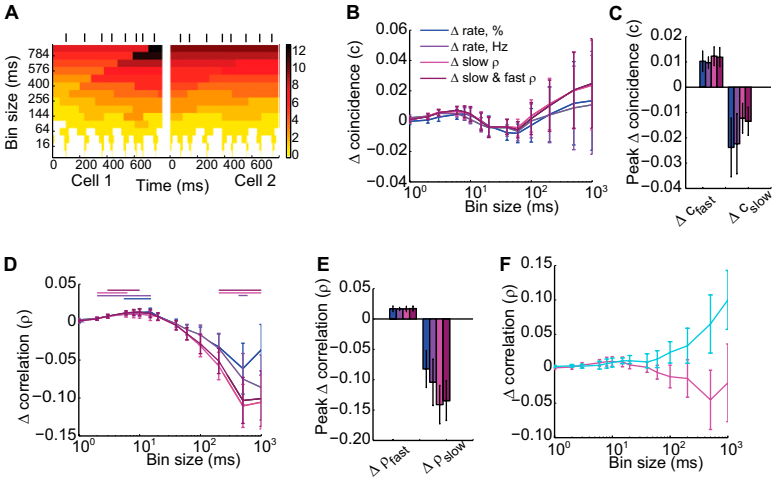

Fig. S3. Measures of coincidence and correlation for the together/separate experiment (Fig. 1). (*A*) Example of spike train binning for two cells. Ticks, above, denote spike times. The heat map denotes spike counts across increasing bin sizes (*y* axis). Observed coincidence (*B*) and correlation (*D*) for four methods of data inclusion are shown. These methods require the following change in the simultaneously recorded condition: an observed percentage of decrease in firing rate (blue), an absolute decrease in firing rate (purple), slow decorrelation (pink), or slow and fast correlation (maroon). Peak increases and decreases in coincidence and correlation for each inclusion method are plotted in *C* and *E*. (*F*) All data from Mg^{2+} (blue) and DHPG (magenta) experiments. Correlation tended to increase in Mg^{2+} experiments because of robust low-frequency changes in spontaneous firing rate that occurred across the slice.

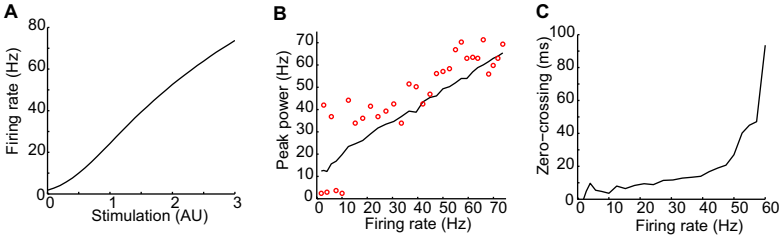

Fig. S4. Relationship between firing rate, power spectrum, and correlation timescales in the two-cell model. (*A*) Frequency-intensity curve for simulated mitral cells. (*B*) Peak of power spectrum of spike trains (black line) and local inputs (red circles) as a function of firing rate in the pair. (*C*) Zero-crossing point of cross-timescale correlation analysis (plotted in Fig. 2*D*) increases with firing rate.

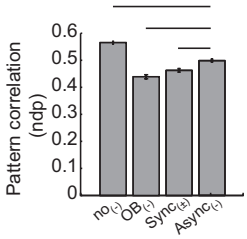

Fig. S5. Normalized dot product (an alternate measure of pattern correlation) is shown for each network model variant. Error bars denote SE, and horizontal bars denote significance.

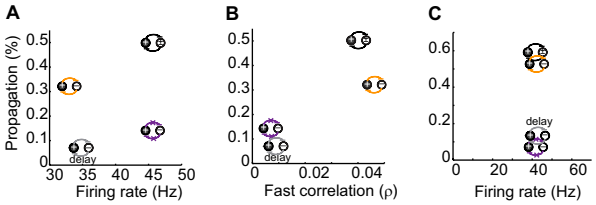

Fig. S6. Comparison of propagation between network model variants. (*A*) Differences in propagation between model variants that are paired for firing rate (olfactory bulb, orange; async$_{(-)}$, gray; no coupling, purple; sync$_{(\pm)}$, black) are attributable to differences in fast-timescale correlation. (*B*) Likewise, in model variants that are paired for fast correlation (no coupling, purple; async$_{(-)}$, gray; olfactory bulb, orange; sync$_{(\pm)}$, black) differences in propagation are attributable to firing rate differences. (*C*) When firing rate is equal for all model variants (by increasing amplitude of current stimulation), async$_{(-)}$ and no coupling have low propagation whereas olfactory bulb and sync$_{(\pm)}$ have high propagation.